18th International Conference on Structural Mechanics in Reactor Technology (SMiRT 18)
Beijing, China, August 7-12, 2005
SMiRT18-KM01-3

# PROBABILISTIC EVALUATION OF NEAR-FIELD GROUND MOTIONS DUE TO BURIED-RUPTURE EARTHQUAKES CAUSED BY UNDEFINED FAULTS

**Shohei Motohashi***
*Japan Nuclear Energy Safety Organization, Japan*
Phone: (81) 3-4511-1571,
Fax: (81) 3-4511-1598
E-mail:
motohashi-shohei@jnes.go.jp

**Katsumi Ebisawa**
*Japan Nuclear Energy Safety Organization, Japan*
Phone: (81) 3-4511-1570,
Fax: (81) 3-4511-1598
E-mail:
ebisawa-katsumi@jnes.go.jp

**Masaharu Sakagami**
*Japan Nuclear Energy Safety Organization, Japan*
Phone: (81) 3-4511-1578,
Fax: (81) 3-4511-1598
E-mail:
sakagami-masaharu@jnes.go.jp

**Kazuo Dan**
*Ohsaki Research Institute, Inc, Japan*
Phone: (81) 3-3508-8011,
Fax: (81) 3-3508-2196
E-mail: dan@ohsaki.co.jp

**Yasuhiro Ohtsuka**
*Kobori Research Complex, Inc, Japan*
Phone: (81) 3-5561-2434,
Fax: (81) 3-5561-2345
E-mail:
yohtsuka@kajima.com

**Takao Kagawa**
*Geo-Research Institute, Japan*
Phone: (81) 6-6539-2975,
Fax: (81) 6-6578-6254
E-mail: kagawa@geor.or.jp

## ABSTRACT

The Nuclear Safety Commission of Japan has been reviewing the current Guideline for Earthquake Resistant Design of Nuclear Power Plants since July 2001. According to recent earthquake research, one of the main issues in the review is the design earthquake motion due to close-by earthquakes caused by undefined faults. This paper proposes a probabilistic method for covering variations of earthquake magnitude and location of undefined faults by strong motion simulation technique based on fault models for scenario earthquakes, and describes probabilistic response spectra due to close-by scenario earthquakes caused by undefined faults. Horizontal uniform hazard spectra evaluated by a hybrid technique are compared with those evaluated by an empirical approach. The response spectra with a damping factor of 5% at 0.02s simulated by the hybrid technique are about 160, 340, 570, and 800 cm/s/s for annual exceedance probabilities of $10^{-3}$, $10^{-4}$, $10^{-5}$, and $10^{-6}$, respectively, which are in good agreement with the response spectra evaluated by the empirical approach. It is also recognized that the response spectrum proposed by Kato et al. (2004) as the upper level of the strong motion records of buried-rupture earthquakes corresponded to the uniform hazard spectra between $10^{-5}$ and $10^{-4}$ in the period range shorter than 0.4s.

**Keywords:** Buried-rupture fault earthquakes, Probabilistic evaluation of strong ground motions, Uniform hazard spectra, Hybrid technique, Empirical approach.

## 1. INTRODUCTION

The 1995 Hyogo-Ken Nambu, Japan, earthquake (Japan Meteorological Agency magnitude $M_J$=7.3) caused the Hanshin-Awaji earthquake disaster, and intensive research on this earthquake and strong motion records promoted the Nuclear Safety Commission of Japan to review the present guideline for earthquake resistant design of nuclear power plants. This disaster also promoted the Japanese Diet to make a new law to establish the Headquarter for Earthquake Research Promotion in the Japanese Government.

According to recent earthquake research, the main issues of the review of the present guidline are strong ground motions due to close-by earthquakes caused by undefined faults, intra-slab earthquakes that generate larger short-period seismic motions than inland earthquakes or subduction earthquakes, and probabilistic evaluation of strong ground motions. This is because the magnitude of close-by earthquakes is specified to be 6.5 in the present guideline while larger-magnitude inland earthquakes caused by undefined faults have actually occurred in Japan, intra-slab earthquakes and their strong motions are not considered explicitly in the present guideline, and determination of a safety goal is expected to become a social requirement for management of nuclear power plants also in Japan.

For the first issue, Kato et al. (2004) recently proposed a design motion based on an upper level of strong motion records on an outcrop due to close-by inland earthquakes caused by undefined faults. Their approach is very convincing because they used actual records, however, it has a limitation with regard to variation of magnitude and location of undefined faults.

Hence, this paper proposed a probabilistic method for covering these variations using a strong motion simulation technique based on fault models for scenario earthquakes, and calculated probabilistic response spectra due to close-by scenario earthquakes caused by undefined faults as seismic hazard uniform spectra. Finally, it compared the probabilistic response spectra with the upper level of the strong motion records proposed by Kato et al. (2004).

## 2. FLOW OF PROCEDURE

We adopted the procedure proposed by Dan et al. (2001) for probabilistic evaluation of near-field ground motions due to buried-rupture earthquakes caused by undefined faults. This procedure consists of four steps: earthquake occurrence modeling, fault rupture scenario modeling, strong motion simulation, and hazard curve calculation.

Figure 1 shows the procedure, where the probability of annual exceedance of horizontal-acceleration response spectra is evaluated for buried-fault rupture earthquakes caused by undefined faults from the relation between the magnitude and the averaged occurrence frequency for inland earthquakes larger than JMA (Japan Meteorological Agency) magnitude 5 in Japan and the relation between the magnitude and the probability of surface breaking analytically estimated from static deformation on the surface (Kagawa et al., 2005). In the seismic-hazard curve calculation, we assumed that the occurrence of buried-fault rupture earthquakes is a Poisson process.

As shown in the upper left of Figure 1, we considered that the distribution of undefined faults around the evaluation point is equivalent to the distribution of evaluation points around the undefined fault. The strong ground motions were simulated at each evaluation point (on seismic bedrock). The evaluation method along the procedure shown in Figure 1 is described in the next section.

## 3. METHODS

### 3.1 Annual Occurrence Frequency of Buried-Fault Rupture Earthquakes

We obtained the following Gutenberg-Richter model of the annual cumulative number of earthquakes per 314km$^2$ in terms of the magnitudes of inland earthquakes from the earthquake catalogue:

$$\log_{10} N(M \geq m) = 2.248 - 0.9189m \qquad \text{Eq. 1}$$

In order to obtain this Eq.1 model, we used 617 Japanese inland earthquakes in a source area of 571,000 km$^2$ with magnitudes larger than 5 and hypocentral depths shallower than 25km in the JMA earthquake catalogue from 1926 to 2002. The epicenters of the earthquake catalogue are shown in Figure 2, and the data and the model of the annual cumulative number of earthquakes are shown in Figure 3.

Kagawa et al. (2005) proposed a probability of surface breaking, $p_{sf}$(M), in terms of magnitude based on the eternal displacement criteria of 5 cm at the fault trace on the bedrock surface after theoretical study on the various

 

strike-slip faults by the analysis of static field changes associated with earthquakes (Okada, 1985). The theoretical probability of surface breaking is shown in Figure 4. The upper part of Figure 4 compares the percentage of surface faults based on the database of actual earthquakes identified by Takemura (1998) with the theoretical probability of surface breaking on strike-slip faults. The open circles indicate that the total number of the events is only one for the corresponding magnitude. The theoretical results confirm that earthquakes of strike-slip faults occur without surface rupture at magnitudes under 6.6 and with surface rupture at magnitudes over 7.3. The lower part of Figure 4 compares the percentage of strike-slip surface faults evaluated from the database of actual earthquakes compiled by Takemura (1998) with the same theoretical result in the upper part of Figure 4. As shown, there is good agreement between them for magnitudes smaller than 6.6 and larger than 6.9.

Consequently, the annual occurrence frequency of buried-fault rupture earthquakes with magnitude M=[m, m+0.1] can be obtained from the annual occurrence frequency of earthquakes and the percentage of surface faults as Eq. 2.

$$\nu(M) = \left[N(M \geq m) - N(M \geq m + 0.1)\right] \times \left[1 - p_{sf}(M)\right]. \text{ (1/year/314km}^2\text{)} \qquad \text{Eq. 2}$$

Figure 5 shows the annual occurrence frequency of buried-fault rupture earthquakes in the evaluation area (dotted line) and that of inland earthquakes (solid line). It is shown that the annual occurrence frequency of buried-fault rupture earthquakes decreased rapidly for magnitudes larger than 7.0.

### 3.2 Fault Rupture Scenarios and Fault Models

We assumed 40 earthquakes scenarios without surface rupture for strike-slip faults with magnitudes of 5.5, 6.0, 6.5, 6.8, 7.1, and 7.3, considering variations of depth (shallow, intermediate, and deep) and stress drop (high, middle, and low) of the asperities. Then, we established fault models for each scenario based on the recipe proposed by Irikura and Miyake (2001) for strong motion prediction.

Figure 6 shows the evaluation area and the strike-slip fault position for magnitudes of 5.5, 6.0, 6.5, 6.8, and 7.3. The earth model (velocity, density, and Q) is shown in Table 1. Figure 7 shows an example of the characterized rupture models of the scenario faults with middle stress drop used in the calculation. The fault parameters of the buried-fault rupture earthquakes of shallow faults are listed in Tables 2, 3, and 4.

### 3.3 Hybrid Technique for Strong Motion Simulation

Strong ground motions on seismic bedrock were simulated for the fault models by a hybrid technique combining a theoretical method and a semi-empirical method (e.g. Kamae et al., 1998; Kagawa, 2004).

This technique adopted the stochastic Green's function method (Kamae et al., 1990) for the short period range and the discrete wave-number method (Bouchon, 1981) for the long period range. Here, $f_{max}$ (cut-off frequency in the high frequency range observed in records) was taken to be 84$^{th}$ percentile (11.9Hz), 50$^{th}$ percentile (7.0Hz), and 16$^{th}$ percentile (4.7Hz) from the spectrum fitting study on actual records totaling 120 cases. In addition, strong ground motions other than sample magnitudes were determined by interpolation or extrapolation between the magnitude range of 5.0 -7.3 by 0.1 step. Furthermore, in order to take account of the distribution of the asperities in the direction of depth, we assumed that the depth of the asperities was distributed uniformly with depth in the seismogenic layer (depth from -3km to -20km).

Finally, the relation between the annual exceedance probability and the uniform hazard spectra was obtained by analyzing acceleration response spectra of about 1,100,000 in total.

### 3.4 Empirical Approach to Strong Motion Simulation

We adopted an earthquake ground motion evaluation method based on an empirical approach proposed by Nishimura et al. (2001) using the parameters of earthquake magnitude, equivalent hypocentral distance, and elastic wave velocity on the ground at the evaluation point. They proposed an empirical approach to evaluate the response spectra of design-basis earthquake ground motions on an outcrop mostly composed of Tertiary or older strata for earthquake resistant design of nuclear power plants.

Noda et al. (2002) found that the response spectra by Nishimura et al. (2001) for shallow inland earthquakes overestimated the observations, and proposed a correction factor. We took into account this correction factor in this study. Strong ground motions on seismic bedrock were also simulated by this empirical approach based on the 40 fault models described in the hybrid technique. Here, we took into account the near-fault rupture directivity effect, too.

 

Finally, the relation between the annual exceedance probability and the uniform hazard spectra was estimated in the same way as the above hybrid technique by using the acceleration response spectra simulated by the empirical approach. Here, a deviation of 0.53 for the natural-logarithmic normal distribution was adopted for the empirically evaluated response spectrum, following to Noda et al. (2002).

## 4. RESULTS

### 4.1 Comparison of Seismic Ground Motions Simulated by Hybrid Technique and Empirical Approach

We simulated strong ground motions from 40 fault models at the 231 (=11x21) positions shown in Figure 6, totaling 9,240 cases.

We first compared the horizontal peak accelerations (values of the acceleration response spectrum with a damping factor of 5% at 0.02s) on the seismic bedrock by the hybrid technique with those simulated by the empirical approach, as shown in Figures 8, 9, and 10 for magnitudes of 6.5, 6.8, and 7.3, respectively, for fault models with shallow faults and middle stress drop according to the fault models of Figure 7. In the hybrid technique, $f_{max}$ was assumed to be 7.0Hz. It is confirmed that the horizontal peak accelerations simulated by both methods are predominant at the position above the larger asperity. Moreover, the near-fault ground motions simulated by the hybrid technique were remarkably larger than those simulated by the empirical approach. The predominance of the near-fault ground motions simulated by the hybrid technique seemed to be affected by the effective stress on the large asperity. However, the overall tendencies of the horizontal peak acceleration contours obtained by the hybrid technique were similar to those obtained by the empirical approach.

We next compared the horizontal-response spectra with a damping factor of 5% simulated by the hybrid technique with those simulated by the empirical approach. Figure 11(1)-(3) compares the average and the average plus/minus the standard deviation of the pseudo velocity response spectra simulated by the hybrid technique in the evaluation area with those simulated by the empirical approach for magnitudes of 6.5, 6.8, and 7.3. Figure 11(4) shows the maximum and the minimum of the pseudo velocity response spectra simulated by the hybrid technique and the empirical approach in the same evaluation area. As shown in Figures 11(1), 11(2), and 11(3), the average and average plus/minus the standard deviation of the response spectra simulated by the hybrid technique were consistent with those simulated by the empirical approach at the same magnitude in the period range shorter than 0.5s. The maximum of the response spectra simulated by the hybrid technique was larger than that simulated by the empirical approach at the same magnitude in the period range shorter than 0.5s, as shown in Figure 11(4). Conversely, the minimum of the response spectra simulated by the hybrid technique was apparently smaller than that simulated by the empirical approach. It was found that the relations between the response spectra simulated by the hybrid technique and the empirical approach in the shorter period range corresponded to the horizontal peak acceleration contours in Figures 8, 9, and 10.

### 4.2 Seismic Hazard Curves and Uniform Hazard Spectra

Figure 12 compares the exceedance probabilities of the horizontal-acceleration response spectra at 0.02s simulated by the hybrid technique for magnitudes of 5.5, 6.0, 6.5, 6.8, and 7.3 with those simulated by the empirical approach. The horizontal response spectra at 0.02s simulated by the hybrid technique were about 30, 40, 60, 80, and 130cm/s/s at $50^{th}$ percentile exceedance probabilities for magnitudes of 5.5, 6.0, 6.5, 6.8, and 7.3, respectively. Those by the empirical approach were about 20, 40, 60, 80, and 140 cm/s/s, respectively. These results are in good agreement, because the average of the response spectra simulated by the hybrid technique is close to that simulated by the empirical approach in the spectral period range shorter than 0.5s, as shown in Figures 11(1), 11(2), and 11(3). However, there was some discrepancy for the exceedance probability lower than the $50^{th}$ percentile. The reason for this discrepancy seems to be that the contour levels of the horizontal peak accelerations of near-fault ground motions simulated by the hybrid technique were different from those by the empirical approach, as shown in Figures 8, 9, and 10.

Figure 13 compares the seismic hazard curves for several spectral periods evaluated by the hybrid technique with those evaluated by the empirical approach. As can be seen, the curves were close at annual exceedance probabilities higher than $10^{-5}$.

The annual exceedance probabilities of the horizontal-response spectra at 0.02s simulated by the hybrid technique and the empirical approach are summarized in Table 5. The horizontal-response spectra with a damping factor of 5% at 0.02s simulated by the hybrid technique were about 160, 340, 570, and 800 cm/s/s at

 

annual exceedance probabilities of $10^{-3}$, $10^{-4}$, $10^{-5}$, and $10^{-6}$, respectively. While those by the empirical response spectrum were about 130, 280, 500, and 800 cm/s/s, respectively.

For a certain annual exceedance probability, the ground motion spectrum (on the seismic bedrock) is extracted from the hazard curves for various spectral periods. These spectra are then plotted at their respective spectral periods to form the uniform hazard spectra.

Using this process, we compared the horizontal-uniform hazard spectra evaluated from the hybrid technique with those evaluated from the empirical approach.

Figure 14 shows two horizontal-uniform hazard spectra at annual exceedance probabilities of $10^{-3}$, $10^{-4}$, $10^{-5}$, and $10^{-6}$; the solid lines are the horizontal-uniform hazard spectra evaluated from the hybrid technique, and the dash-dotted lines are those evaluated from the empirical approach. The uniform hazard spectra evaluated by the hybrid technique show good agreement with those evaluated by the empirical approach, except that the uniform hazard spectra for the annual exceedance probability of $10^{-6}$ in the period range longer than 0.5s are different.

### 4.3 Comparison of Uniform Hazard Spectra and Earthquake Ground Motions by Undefined Faults in Upper Crust

As previously stated, Kato et al. (2004) recently proposed an upper level of strong motion records on an outcrop due to inland earthquakes caused by undefined faults. Kato et al. (2004) investigated 41 earthquakes that occurred in the upper crust with a moment magnitude from 5.6 to 7.5, and used 30 strong motion records observed at 12 stations on rock sites from 9 earthquakes to determine the upper strong motion level for undefined faults. The estimated upper level of peak ground acceleration is 450cm/s/s on seismic bedrock. On the other hand, Kato et al. (2004) referred to a possibility of occurrence of strong ground motions exceeding their estimated upper strong motion and the importance of probabilistic evaluation of strong motion caused by undefined faults.

Finally, the probabilistic response spectra by the hybrid technique and the empirical approach were compared with the upper level of the response spectra proposed by Kato et al (2004) in Figure 15. As shown, the annual probability of exceeding the upper level was evaluated to be between $10^{-5}$ and $10^{-4}$ in the period range shorter than 0.4s.

## 5. CONCLUSIONS

We have proposed a method for covering the variation of magnitude and location of undefined faults by a strong motion simulation technique based on fault models for scenario earthquakes, and calculated probabilistic response spectra due to close-by scenario earthquakes caused by undefined faults based on occurrence models.

The horizontal-uniform hazard spectra evaluated by this hybrid technique were compared with those evaluated by the empirical approach. As a result, the response spectra with a damping factor of 5% at 0.02s simulated by the hybrid technique were about 160, 340, 570, and 800cm/s/s at annual exceedance probabilities of $10^{-3}$, $10^{-4}$, $10^{-5}$, and $10^{-6}$, respectively, which were in good agreement with the response spectra evaluated by the empirical approach.

It was also recognized that the response spectrum proposed by Kato et al. (2004) as the upper level of the strong motion records for earthquakes from undefined faults corresponded to the uniform hazard spectra between $10^{-5}$ and $10^{-4}$ in the short period range.

## 6. ACKNOWLEDGMENTS

The Ministry of Economy, Trade and Industry, Japan sponsored this research. We would like to express our appreciation to Dr. Sci. Kojiro Irikura, Vice President of Kyoto University, for his guidance in the strong motion simulation technique based on asperity models. We would also like to thank Dr. Takahide Watanabe, Mr. Toshihiko Okumura, and Mr. Yasuhiro Ohashi of Ohsaki Research Institute, Inc. and Dr. Sci. Masayuki Takemura, Dr. Minoru Kanechika, and Dr. Tomonori Ikeura of Kobori Research Complex, Inc. for fruitful discussions.

 

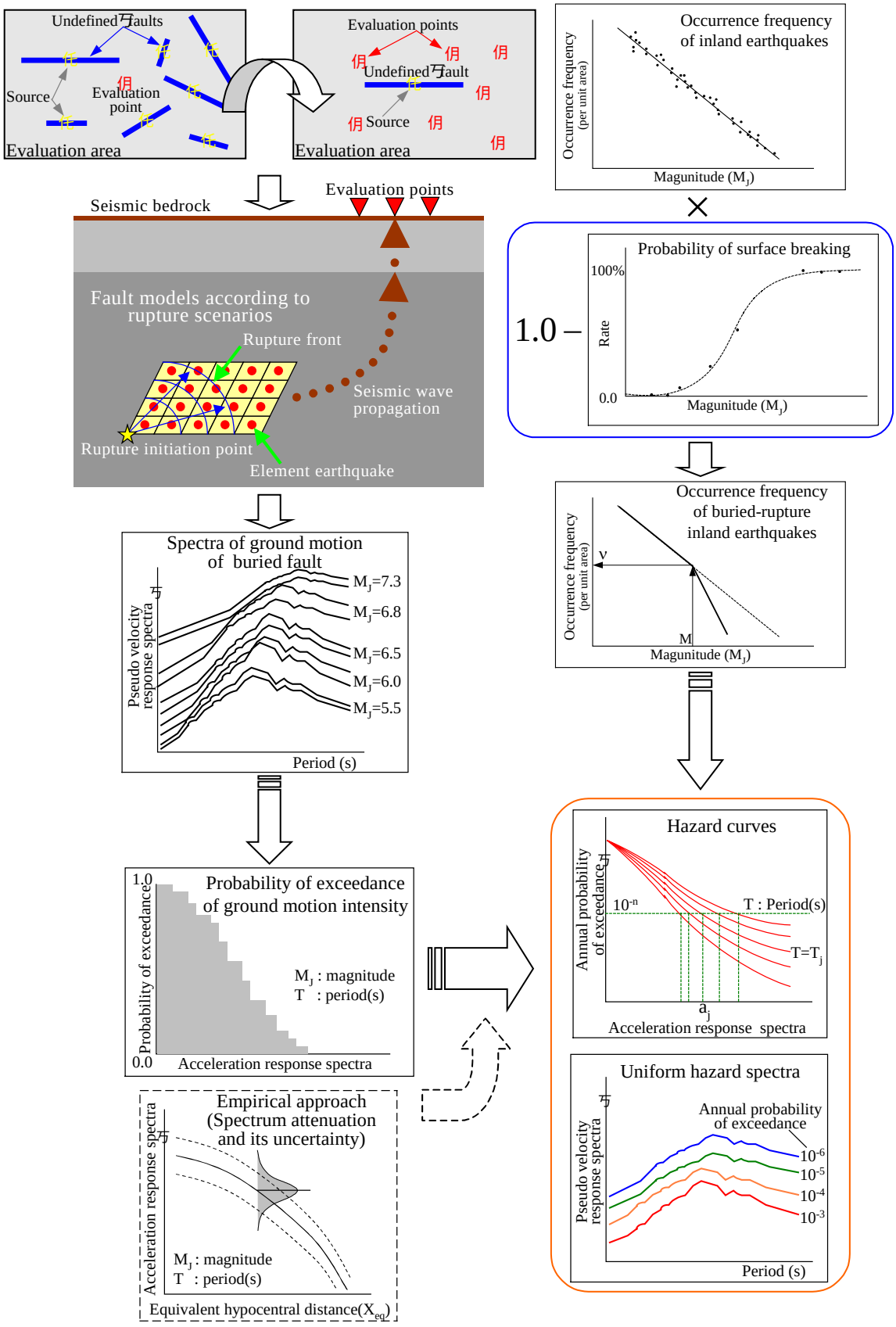


*Figure 1 Flow chart of procedure.*


*Figure 2 Source area model and distribution of epicenters of inland earthquakes*

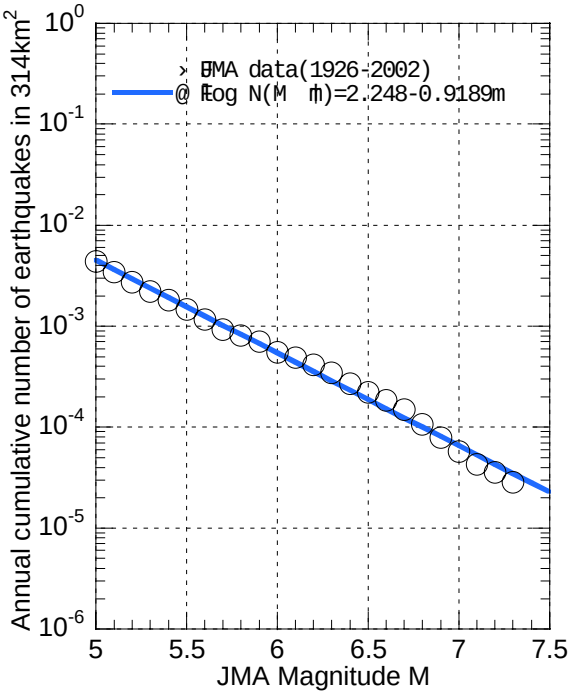


*Figure 3 Annual cumulative number of occurrence of inland earthquakes in 314 km$^2$*

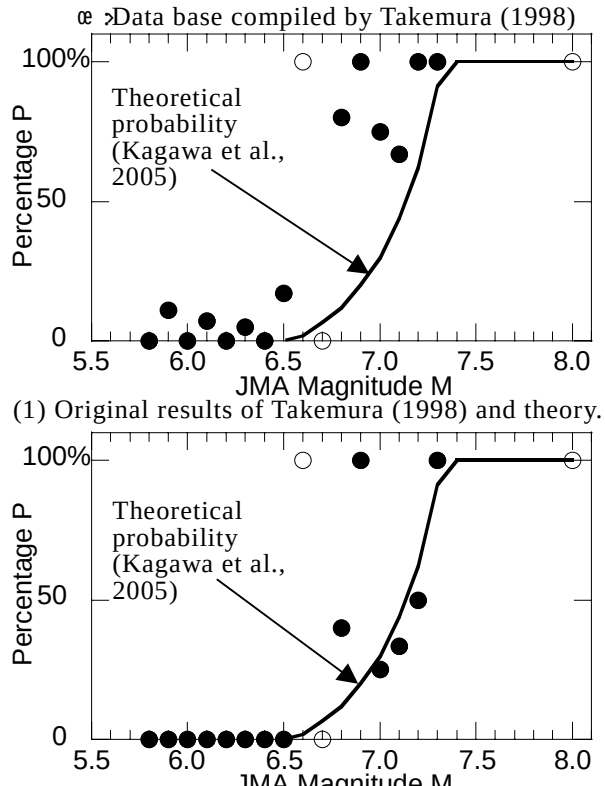


(1) Original results of Takemura (1998) and theory.

(2) Strike-slip surface faults evaluated based on the database of Takemura (1998) and theory.

*Figure 4 Probability of surface breaking. (after data base of Takemura (1998))*

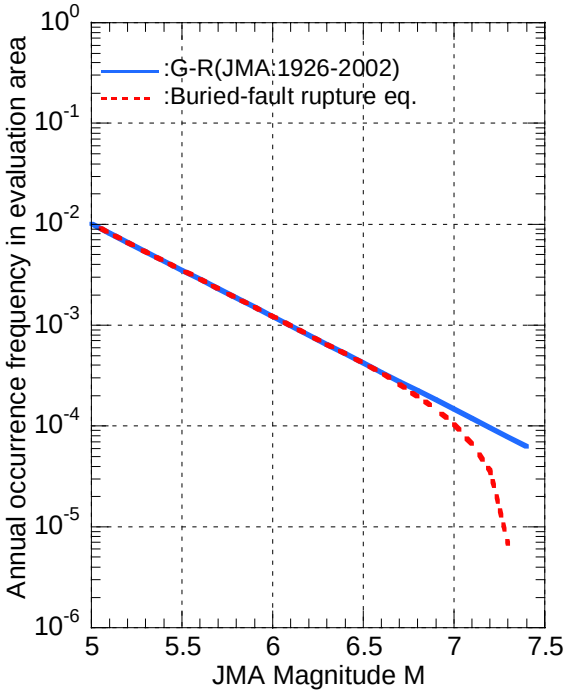


*Figure 5 Annual occurrence frequency of buried-fault rupture earthquakes in the evaluation area (3696 km$^2$).*

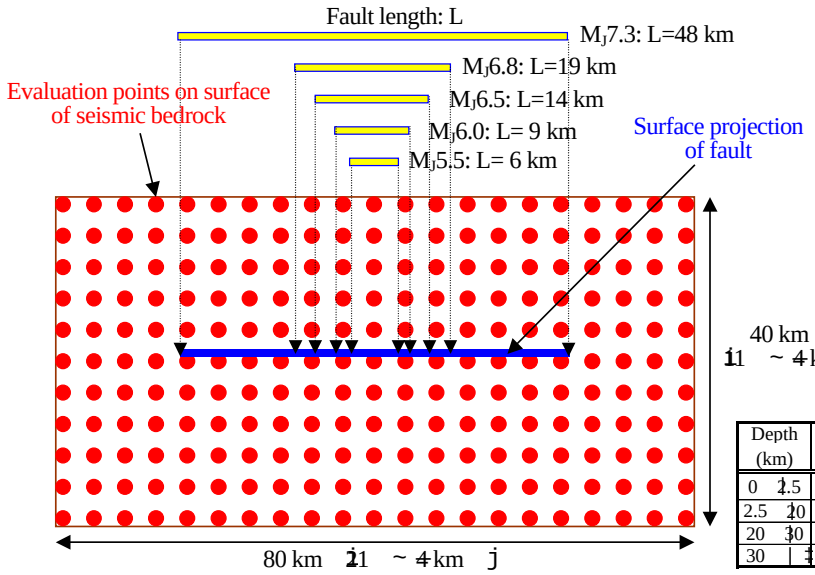


*Figure 6 Evaluation area and fault position.*

*Table 1 Earth model for strong motion simulation.*

| Depth (km) | $V_P$ (km/s) | $V_S$ (km/s) | $\rho$ (kN/m$^3$) | Q | |
|---|---|---|---|---|---|
| | | | | f 1.0 Hz | f >1.0 Hz |
| 0 2.5 | 4.5 | 2.6 | 24 | 200 | $130\ f^{0.77}$ |
| 2.5 20 | 6.0 | 3.5 | 27 | 400 | |
| 20 30 | 6.7 | 3.9 | 28 | 500 | |
| 30 | 7.7 | 4.4 | 32 | 800 | |

*Table 2 Fault parameters of earthquake of shallow fault and high stress drop.*

| Parameters | | | Japan Meteorological Agency magnitude | | | | |
|---|---|---|---|---|---|---|---|
| | | | 5.5 | 6.0 | 6.5 | 6.8 | 7.3 |
| Strike | | | N090E (EW direction) | | | | |
| Dip | | | 90 (vertical) | | | | |
| Rake | | | 0 (left-lateral strike-slip) | | | | |
| Moment magnitude | $M_W$ | | 5.5 | 5.9 | 6.3 | 6.5 | 6.9 |
| Seismic moment | $M_0$ | ? $10^{-7}$[N m] | 2.00E+24 | 7.94E+24 | 3.16E+25 | 7.24E+25 | 2.88E+26 |
| Upper depth of the fault | | [km] | 3 | 3 | 3 | 3 | 3 |
| Lower depth of the fault | | [km] | 8 | 11 | 16 | 20 | 20 |
| Area of the entire fault | $S$ | [km$^2$] | 29.3 | 73.6 | 185.0 | 321.5 | 807.6 |
| Mean depth of the larger asperity | $H$ | [km] | 4.0 | 4.5 | 5.5 | 6.0 | 13.0 |
| Short-period level | $A$ | ? $10^{-7}$[N m/s$^2$] | 3.74E+25 | 5.93E+25 | 9.40E+25 | 1.24E+26 | 1.96E+26 |
| Area of the asperities | $Sasp$ | [km$^2$] | 4.7 | 11.8 | 29.6 | 51.4 | 129.2 |
| Area of the larger asperity | $S_1$ | [km$^2$] | 3.3 | 8.2 | 20.7 | 36.0 | 90.4 |
| Area of the smaller asperity | $S_2$ | [km$^2$] | 1.4 | 3.5 | 8.9 | 15.4 | 38.8 |
| Area of the background | $S_b$ | [km$^2$] | 24.6 | 61.9 | 155.4 | 270.1 | 678.3 |
| Fault length | $L$ | [km] | 6 | 9 | 14 | 19 | 48 |
| Fault width | $W$ | [km] | 5 | 8 | 13 | 17 | 17 |
| Length of the larger asperity | $L_1$ | [km] | 2 | 3 | 4 | 6 | 9 |
| Width of the larger asperity | $W_1$ | [km] | 2 | 3 | 5 | 6 | 10 |
| Length of the smaller asperity | $L_2$ | [km] | 1 | 2 | 3 | 4 | 6 |
| Width of the smaller asperity | $W_2$ | [km] | 1 | 2 | 3 | 4 | 6 |
| Upper depth of the larger asperity | | [km] | 3 | 3 | 3 | 4 | 8 |
| Rupture initiation point | | | Deeper point in the center of the fault | | | | |
| Rupture propagation velocity | | [km/s] | 2.7 | | | | |
| Rupture propagation mode | | | Radial | | | | |
| Rise time | $\tau$ | [s] | 0.26 | 0.41 | 0.64 | 0.85 | 1.34 |
| Shear-wave velocity | $\beta$ | [km/s] | 3.5 | | | | |
| Rigidity | $\mu$ | ? $10^{-1}$[N/m$^2$] | 3.31E+11 | | | | |
| Averaged slip on the entire fault | $D$ | [cm] | 21 | 33 | 52 | 68 | 108 |
| Slip ratio | $\gamma$ | | 1.96 | | | | |
| Slip on the larger asperity | $D_1$ | [cm] | 45 | 71 | 113 | 149 | 236 |
| Slip on the smaller asperity | $D_2$ | [cm] | 29 | 47 | 74 | 97 | 154 |
| Slip on the background | $D_b$ | [cm] | 17 | 27 | 42 | 56 | 88 |
| Seismic moment of the larger asperity | $M_{01}$ | ? $10^{-7}$[N m] | 4.89E+23 | 1.95E+24 | 7.74E+24 | 1.77E+25 | 7.06E+25 |
| Seismic moment of the smaller asperity | $M_{02}$ | ? $10^{-7}$[N m] | 1.37E+23 | 5.46E+23 | 2.17E+24 | 4.98E+24 | 1.98E+25 |
| Seismic moment of the background | $M_{0b}$ | ? $10^{-7}$[N m] | 1.37E+24 | 5.45E+24 | 2.17E+25 | 4.97E+25 | 1.98E+26 |
| Effective stress on the larger asperity | $\sigma_1$ | ? $10^{-1}$[MPa] | 191 | 191 | 191 | 191 | 191 |
| Effective stress on the smaller asperity | $\sigma_2$ | ? $10^{-1}$[MPa] | 191 | 191 | 191 | 191 | 191 |
| Effective stress on the background | $\sigma_b$ | ? $10^{-1}$[MPa] | 24 | 24 | 24 | 24 | 24 |
| Length of the calculation region | | [km] | 80 | | | | |
| Width of the calculation region | | [km] | 40 | | | | |

*Table 3 Fault parameters of earthquake of shallow fault and middle stress drop.*

| Parameters | | | Japan Meteorological Agency magnitude | | | | |
|---|---|---|---|---|---|---|---|
| | | | 5.5 | 6.0 | 6.5 | 6.8 | 7.3 |
| Strike | | | N090E (EW direction) | | | | |
| Dip | | | 90 (vertical) | | | | |
| Rake | | | 0 (left-lateral strike-slip) | | | | |
| Moment magnitude | $M_W$ | | 5.5 | 5.9 | 6.3 | 6.5 | 6.9 |
| Seismic moment | $M_0$ | ? $10^{-7}$[N m] | 2.00E+24 | 7.94E+24 | 3.16E+25 | 7.24E+25 | 2.88E+26 |
| Upper depth of the fault | | [km] | 3 | 3 | 3 | 3 | 3 |
| Lower depth of the fault | | [km] | 8 | 11 | 16 | 20 | 20 |
| Area of the entire fault | $S$ | [$km^2$] | 29.3 | 73.6 | 185.0 | 321.5 | 807.6 |
| Mean depth of the larger asperity | $H$ | [km] | 4.0 | 5.0 | 6.0 | 8.5 | 14.5 |
| Short-period level | $A$ | ? $10^{-7}$[N m/$s^2$] | 3.16E+25 | 5.01E+25 | 7.94E+25 | 1.05E+26 | 1.66E+26 |
| Area of the asperities | $Sasp$ | [$km^2$] | 6.5 | 16.2 | 40.7 | 70.7 | 177.7 |
| Area of the larger asperity | $S_1$ | [$km^2$] | 4.5 | 11.3 | 28.5 | 49.5 | 124.4 |
| Area of the smaller asperity | $S_2$ | [$km^2$] | 1.9 | 4.9 | 12.2 | 21.2 | 53.3 |
| Area of the background | $S_b$ | [$km^2$] | 22.9 | 57.4 | 144.3 | 250.8 | 629.9 |
| Fault length | $L$ | [km] | 6 | 9 | 14 | 19 | 48 |
| Fault width | $W$ | [km] | 5 | 8 | 13 | 17 | 17 |
| Length of the larger asperity | $L_1$ | [km] | 2 | 3 | 5 | 7 | 11 |
| Width of the larger asperity | $W_1$ | [km] | 2 | 4 | 6 | 7 | 11 |
| Length of the smaller asperity | $L_2$ | [km] | 1 | 2 | 3 | 4 | 7 |
| Width of the smaller asperity | $W_2$ | [km] | 2 | 2 | 4 | 5 | 8 |
| Upper depth of the larger asperity | | [km] | 3 | 3 | 3 | 5 | 9 |
| Rupture initiation point | | | Deeper point in the center of the fault | | | | |
| Rupture propagation velocity | | [km/s] | 2.7 | | | | |
| Rupture propagation mode | | | Radial | | | | |
| Rise time | $\tau$ | [s] | 0.26 | 0.41 | 0.64 | 0.85 | 1.34 |
| Shear-wave velocity | $\beta$ | [km/s] | 3.5 | | | | |
| Rigidity | $\mu$ | ? $10^{-1}$[N/$m^2$] | 3.31E+11 | | | | |
| Averaged slip on the entire fault | $D$ | [cm] | 21 | 33 | 52 | 68 | 108 |
| Slip ratio | $\gamma$ | | 1.96 | | | | |
| Slip on the larger asperity | $D_1$ | [cm] | 45 | 71 | 113 | 149 | 236 |
| Slip on the smaller asperity | $D_2$ | [cm] | 29 | 47 | 74 | 97 | 154 |
| Slip on the background | $D_b$ | [cm] | 15 | 24 | 38 | 50 | 79 |
| Seismic moment of the larger asperity | $M_{01}$ | ? $10^{-7}$[N m] | 6.72E+23 | 2.67E+24 | 1.06E+25 | 2.44E+25 | 9.71E+25 |
| Seismic moment of the smaller asperity | $M_{02}$ | ? $10^{-7}$[N m] | 1.89E+23 | 7.50E+23 | 2.99E+24 | 6.84E+24 | 2.72E+25 |
| Seismic moment of the background | $M_{0b}$ | ? $10^{-7}$[N m] | 1.13E+24 | 4.52E+24 | 1.80E+25 | 4.12E+25 | 1.64E+26 |
| Effective stress on the larger asperity | $\sigma_1$ | ? $10^{-1}$[MPa] | 139 | 139 | 139 | 139 | 139 |
| Effective stress on the smaller asperity | $\sigma_2$ | ? $10^{-1}$[MPa] | 139 | 139 | 139 | 139 | 139 |
| Effective stress on the background | $\sigma_b$ | ? $10^{-1}$[MPa] | 18 | 18 | 18 | 18 | 18 |

*Table 4 Fault parameters of earthquake of shallow fault and low stress drop.*

| Parameters | | | Japan Meteorological Agency magnitude | | | | |
|---|---|---|---|---|---|---|---|
| | | | 5.5 | 6.0 | 6.5 | 6.8 | 7.1 |
| Strike | | | N090E (EW direction) | | | | |
| Dip | | | 90 (vertical) | | | | |
| Rake | | | 0 (left-lateral strike-slip) | | | | |
| Moment magnitude | $M_W$ | | 5.5 | 5.9 | 6.3 | 6.5 | 6.7 |
| Seismic moment | $M_0$ | ? $10^{-7}$[N m] | 2.00E+24 | 7.94E+24 | 3.16E+25 | 7.24E+25 | 1.66E+26 |
| Upper depth of the fault | | [km] | 3 | 3 | 3 | 3 | 3 |
| Lower depth of the fault | | [km] | 8 | 11 | 16 | 20 | 20 |
| Area of the entire fault | $S$ | [$km^2$] | 29.3 | 73.6 | 185.0 | 321.5 | 558.7 |
| Mean depth of the larger asperity | $H$ | [km] | 4.5 | 5.0 | 7.0 | 9.0 | 13.5 |
| Short-period level | $A$ | ? $10^{-7}$[N m/$s^2$] | 2.77E+25 | 4.40E+25 | 6.97E+25 | 9.19E+25 | 1.21E+26 |
| Area of the asperities | $Sasp$ | [$km^2$] | 8.2 | 20.6 | 51.8 | 90.0 | 156.4 |
| Area of the larger asperity | $S_1$ | [$km^2$] | 5.7 | 14.4 | 36.3 | 63.0 | 109.5 |
| Area of the smaller asperity | $S_2$ | [$km^2$] | 2.5 | 6.2 | 15.5 | 27.0 | 46.9 |
| Area of the background | $S_b$ | [$km^2$] | 21.1 | 53.0 | 133.2 | 231.5 | 402.3 |
| Fault length | $L$ | [km] | 6 | 9 | 14 | 19 | 33 |
| Fault width | $W$ | [km] | 5 | 8 | 13 | 17 | 17 |
| Length of the larger asperity | $L_1$ | [km] | 2 | 4 | 6 | 8 | 10 |
| Width of the larger asperity | $W_1$ | [km] | 3 | 4 | 6 | 8 | 11 |
| Length of the smaller asperity | $L_2$ | [km] | 1 | 2 | 4 | 5 | 7 |
| Width of the smaller asperity | $W_2$ | [km] | 2 | 3 | 4 | 5 | 7 |
| Upper depth of the larger asperity | | [km] | 3 | 3 | 4 | 5 | 8 |
| Rupture initiation point | | | Deeper point in the center of the fault | | | | |
| Rupture propagation velocity | | [km/s] | 2.7 | | | | |
| Rupture propagation mode | | | Radial | | | | |
| Rise time | $\tau$ | [s] | 0.26 | 0.41 | 0.64 | 0.85 | 1.12 |
| Shear-wave velocity | $\beta$ | [km/s] | 3.5 | | | | |
| Rigidity | $\mu$ | ? $10^{-1}$[N/$m^2$] | 3.31E+11 | | | | |
| Averaged slip on the entire fault | $D$ | [cm] | 21 | 33 | 52 | 68 | 90 |
| Slip ratio | $\gamma$ | | 1.96 | | | | |
| Slip on the larger asperity | $D_1$ | [cm] | 45 | 71 | 113 | 149 | 196 |
| Slip on the smaller asperity | $D_2$ | [cm] | 29 | 47 | 74 | 97 | 128 |
| Slip on the background | $D_b$ | [cm] | 13 | 20 | 32 | 43 | 56 |
| Seismic moment of the larger asperity | $M_{01}$ | ? $10^{-7}$[N m] | 8.55E+23 | 3.40E+24 | 1.36E+25 | 3.10E+25 | 7.11E+25 |
| Seismic moment of the smaller asperity | $M_{02}$ | ? $10^{-7}$[N m] | 2.40E+23 | 9.55E+23 | 3.80E+24 | 8.71E+24 | 2.00E+25 |
| Seismic moment of the background | $M_{0b}$ | ? $10^{-7}$[N m] | 9.00E+23 | 3.58E+24 | 1.43E+25 | 3.27E+25 | 7.49E+25 |
| Effective stress on the larger asperity | $\sigma_1$ | ? $10^{-1}$[MPa] | 109 | 109 | 109 | 109 | 109 |
| Effective stress on the smaller asperity | $\sigma_2$ | ? $10^{-1}$[MPa] | 109 | 109 | 109 | 109 | 109 |
| Effective stress on the background | $\sigma_b$ | ? $10^{-1}$[MPa] | 14 | 14 | 14 | 14 | 14 |

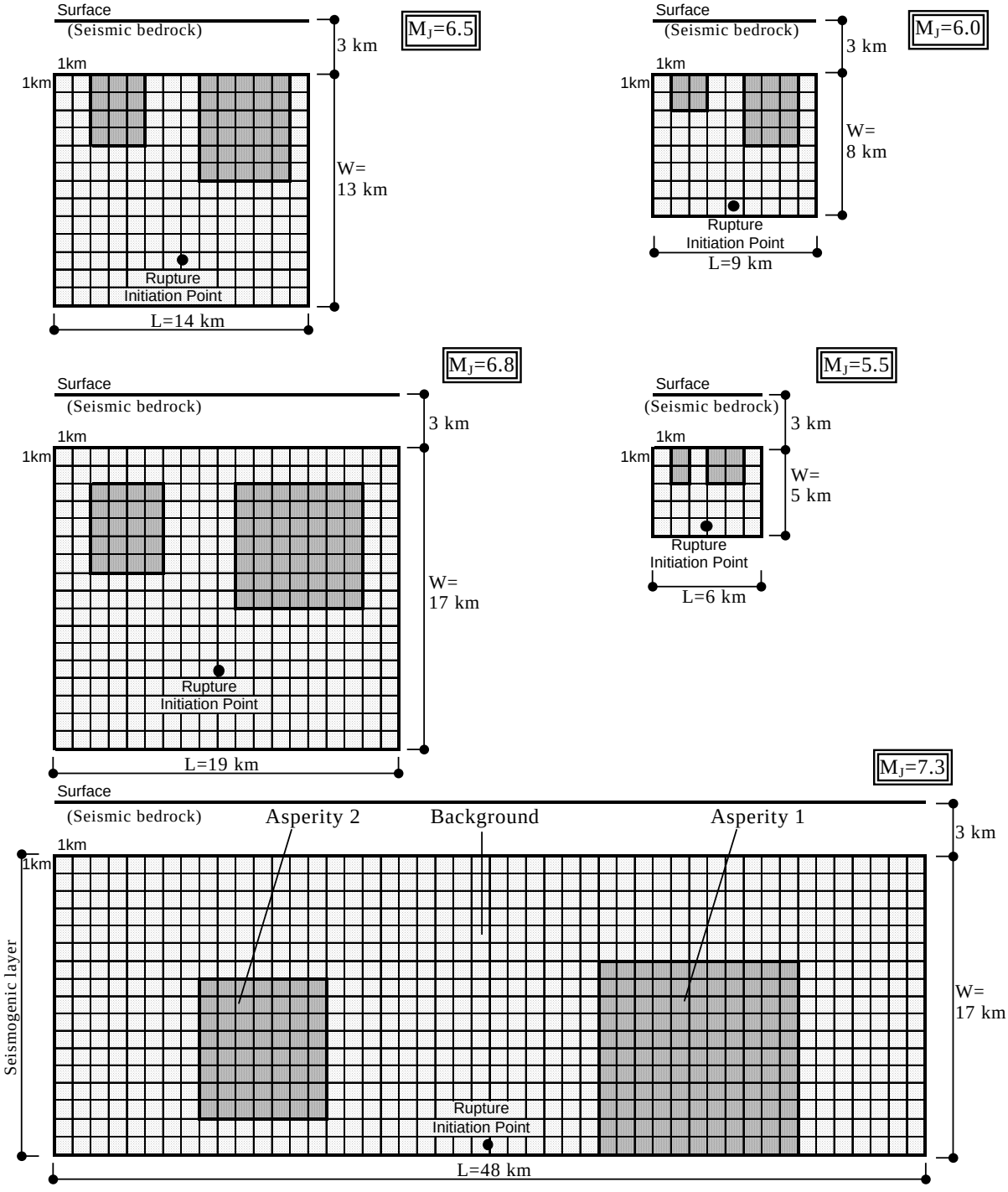


*Figure 7 Fault models for earthquakes of shallow fault and middle stress drop.*

| M65(FN) | -400 | -360 | -320 | -280 | -240 | -200 | -160 | -120 | -80 | -40 | 00 | 40 | 80 | 120 | 160 | 200 | 240 | 280 | 320 | 360 | 40(km) |
|---|---|---|---|---|---|---|---|---|---|---|---|---|---|---|---|---|---|---|---|---|---|
| 200 | 141 | 114 | 190 | 296 | 252 | 554 | 898 | 680 | 993 | 1275 | 1000 | 977 | 873 | 760 | 671 | 547 | 379 | 297 | 236 | 210 | 188 |
| 160 | 133 | 136 | 161 | 254 | 267 | 536 | 625 | 1053 | 896 | 1026 | 1532 | 1144 | 1124 | 1035 | 797 | 502 | 539 | 288 | 213 | 189 | 116 |
| 120 | 141 | 150 | 196 | 296 | 438 | 422 | 570 | 668 | 1357 | 1937 | 1930 | 1419 | 1466 | 1226 | 953 | 574 | 391 | 271 | 222 | 158 | 136 |
| 80 | 122 | 188 | 216 | 267 | 344 | 375 | 505 | 1237 | 1429 | 2105 | 2776 | 2280 | 1569 | 1816 | 1103 | 566 | 448 | 358 | 284 | 179 | 165 |
| 40 | 156 | 206 | 191 | 232 | 369 | 491 | 757 | 1430 | 2304 | 3418 | 4115 | 3572 | 4766 | 2353 | 872 | 735 | 577 | 368 | 275 | 210 | 158 |
| 00 | 134 | 174 | 226 | 306 | 436 | 521 | 646 | 1608 | 2725 | 3751 | 6267 | 7100 | 6327 | 3051 | 1111 | 784 | 712 | 396 | 282 | 260 | 154 |
| -40 | 145 | 189 | 204 | 246 | 319 | 425 | 851 | 1087 | 2583 | 2400 | 2185 | 2950 | 2795 | 2030 | 1666 | 739 | 438 | 350 | 299 | 202 | 170 |
| -80 | 135 | 176 | 218 | 242 | 227 | 442 | 556 | 1242 | 1232 | 2134 | 1846 | 1494 | 1641 | 1501 | 1165 | 542 | 388 | 283 | 201 | 142 | 191 |
| -120 | 154 | 134 | 157 | 210 | 374 | 410 | 536 | 1069 | 1152 | 1265 | 1262 | 1047 | 1417 | 1011 | 863 | 651 | 432 | 299 | 211 | 174 | 165 |
| -160 | 113 | 181 | 212 | 291 | 395 | 508 | 678 | 844 | 1094 | 945 | 1243 | 1028 | 1205 | 962 | 662 | 577 | 309 | 294 | 205 | 156 | 181 |
| -200 | 160 | 194 | 240 | 259 | 308 | 384 | 728 | 921 | 778 | 675 | 899 | 796 | 691 | 889 | 812 | 547 | 495 | 216 | 212 | 206 | 171 |

(a) Fault normal

| M65(FP) | -400 | -360 | -320 | -280 | -240 | -200 | -160 | -120 | -80 | -40 | 00 | 40 | 80 | 120 | 160 | 200 | 240 | 280 | 320 | 360 | 40(km) |
|---|---|---|---|---|---|---|---|---|---|---|---|---|---|---|---|---|---|---|---|---|---|
| 200 | 235 | 216 | 321 | 338 | 453 | 344 | 452 | 521 | 494 | 534 | 772 | 564 | 556 | 464 | 409 | 422 | 564 | 425 | 353 | 298 | 335 |
| 160 | 344 | 327 | 380 | 491 | 417 | 488 | 893 | 623 | 610 | 843 | 1040 | 755 | 794 | 661 | 551 | 574 | 498 | 488 | 437 | 325 | 283 |
| 120 | 230 | 458 | 553 | 578 | 647 | 745 | 696 | 1006 | 858 | 1335 | 1521 | 1250 | 1158 | 1327 | 950 | 786 | 596 | 487 | 406 | 291 | 315 |
| 80 | 322 | 396 | 545 | 384 | 642 | 777 | 901 | 1277 | 2771 | 2145 | 2493 | 2527 | 2995 | 1422 | 1247 | 740 | 786 | 601 | 412 | 344 | 363 |
| 40 | 349 | 435 | 373 | 461 | 603 | 625 | 1000 | 1187 | 2516 | 4156 | 3902 | 6560 | 4703 | 2186 | 1063 | 917 | 732 | 575 | 481 | 397 | 322 |
| 00 | 342 | 446 | 410 | 418 | 450 | 714 | 1173 | 1252 | 1696 | 2485 | 3405 | 5215 | 2929 | 2094 | 1017 | 898 | 878 | 606 | 443 | 392 | 327 |
| -40 | 289 | 303 | 349 | 631 | 507 | 695 | 886 | 1620 | 1602 | 2792 | 2504 | 3371 | 2745 | 2766 | 1234 | 729 | 734 | 603 | 538 | 319 | 324 |
| -80 | 295 | 429 | 405 | 524 | 582 | 771 | 1153 | 771 | 1345 | 1505 | 1692 | 2242 | 1428 | 1755 | 1309 | 772 | 827 | 644 | 414 | 274 | 244 |
| -120 | 368 | 407 | 442 | 384 | 459 | 644 | 856 | 669 | 643 | 931 | 1174 | 1074 | 1128 | 862 | 672 | 620 | 754 | 468 | 306 | 309 | 329 |
| -160 | 254 | 246 | 315 | 349 | 468 | 540 | 567 | 507 | 584 | 755 | 725 | 863 | 549 | 471 | 511 | 401 | 423 | 390 | 348 | 284 | 275 |
| -200 | 291 | 429 | 327 | 319 | 358 | 371 | 387 | 444 | 405 | 559 | 709 | 636 | 510 | 349 | 432 | 373 | 352 | 326 | 413 | 291 | 227 |

(b) Fault parallel

(1) Hybrid technique ($f_{max}$=7.0Hz)

| M65sh | -400 | -360 | -320 | -280 | -240 | -200 | -160 | -120 | -80 | -40 | 00 | 40 | 80 | 120 | 160 | 200 | 240 | 280 | 320 | 360 | 40(km) |
|---|---|---|---|---|---|---|---|---|---|---|---|---|---|---|---|---|---|---|---|---|---|
| 200 | 272 | 309 | 353 | 407 | 458 | 515 | 578 | 646 | 711 | 763 | 793 | 792 | 759 | 703 | 636 | 567 | 504 | 448 | 396 | 344 | 301 |
| 160 | 287 | 329 | 381 | 439 | 500 | 573 | 660 | 759 | 862 | 951 | 1005 | 1004 | 947 | 852 | 745 | 645 | 559 | 487 | 428 | 370 | 320 |
| 120 | 300 | 347 | 406 | 466 | 540 | 633 | 751 | 898 | 1064 | 1223 | 1329 | 1332 | 1221 | 1048 | 875 | 729 | 614 | 524 | 454 | 393 | 336 |
| 80 | 310 | 361 | 423 | 489 | 574 | 687 | 841 | 1053 | 1328 | 1607 | 1807 | 1831 | 1617 | 1296 | 1014 | 809 | 662 | 555 | 474 | 411 | 349 |
| 40 | 315 | 369 | 433 | 503 | 595 | 723 | 909 | 1191 | 1614 | 2093 | 2485 | 2608 | 2108 | 1533 | 1125 | 865 | 694 | 574 | 487 | 420 | 356 |
| 00 | 317 | 370 | 435 | 505 | 600 | 731 | 924 | 1228 | 1709 | 2301 | 2774 | 2988 | 2296 | 1594 | 1152 | 878 | 701 | 578 | 489 | 422 | 358 |
| -40 | 313 | 365 | 429 | 497 | 586 | 708 | 880 | 1129 | 1479 | 1839 | 2126 | 2182 | 1856 | 1427 | 1076 | 841 | 681 | 566 | 481 | 417 | 353 |
| -80 | 305 | 354 | 416 | 478 | 558 | 661 | 798 | 974 | 1188 | 1404 | 1548 | 1557 | 1407 | 1167 | 945 | 770 | 639 | 540 | 465 | 403 | 343 |
| -120 | 294 | 338 | 394 | 453 | 520 | 603 | 705 | 825 | 956 | 1074 | 1149 | 1149 | 1070 | 943 | 808 | 687 | 587 | 506 | 441 | 382 | 329 |
| -160 | 280 | 319 | 367 | 424 | 479 | 543 | 618 | 699 | 781 | 849 | 889 | 888 | 845 | 772 | 688 | 605 | 531 | 468 | 414 | 357 | 311 |
| -200 | 264 | 298 | 339 | 387 | 437 | 487 | 541 | 597 | 650 | 691 | 714 | 713 | 688 | 644 | 589 | 532 | 478 | 429 | 377 | 330 | 291 |

(2) Empirical approach

*Figure 8 Contour of estimated peak accelerations on seismic bedrock for $M_J$=6.5 with shallow fault and middle stress drop.*

| M68(FN) | -400 | -360 | -320 | -280 | -240 | -200 | -160 | -120 | -80 | -40 | 00 | 40 | 80 | 120 | 160 | 200 | 240 | 280 | 320 | 360 | 40(km) |
|---|---|---|---|---|---|---|---|---|---|---|---|---|---|---|---|---|---|---|---|---|---|
| 200 | 215 | 267 | 331 | 380 | 354 | 647 | 979 | 1385 | 1093 | 1206 | 1260 | 1117 | 1412 | 956 | 929 | 845 | 635 | 594 | 390 | 293 | 192 |
| 160 | 226 | 243 | 394 | 526 | 607 | 682 | 873 | 1104 | 1384 | 1265 | 1207 | 1189 | 1708 | 1725 | 874 | 828 | 618 | 508 | 340 | 273 | 265 |
| 120 | 308 | 332 | 456 | 458 | 607 | 827 | 1068 | 1312 | 1562 | 1745 | 1503 | 2024 | 1366 | 1364 | 1128 | 957 | 809 | 663 | 493 | 411 | 263 |
| 80 | 333 | 463 | 564 | 520 | 857 | 949 | 1528 | 1936 | 2458 | 1927 | 1947 | 1990 | 2343 | 1317 | 1530 | 1416 | 799 | 690 | 672 | 390 | 356 |
| 40 | 317 | 475 | 442 | 546 | 683 | 1144 | 1436 | 3214 | 3575 | 4119 | 2989 | 3836 | 4081 | 2425 | 2249 | 1497 | 1264 | 806 | 647 | 457 | 426 |
| 00 | 323 | 495 | 504 | 690 | 675 | 852 | 2434 | 3431 | 2980 | 2938 | 2883 | 5281 | 4163 | 3717 | 2351 | 1598 | 1232 | 841 | 642 | 474 | 354 |
| -40 | 296 | 430 | 521 | 530 | 600 | 1048 | 1416 | 2027 | 2566 | 2925 | 2443 | 2205 | 2412 | 1714 | 1932 | 1812 | 941 | 916 | 555 | 533 | 446 |
| -80 | 284 | 322 | 442 | 459 | 556 | 729 | 1130 | 1736 | 1233 | 1751 | 1741 | 1785 | 1528 | 1584 | 1196 | 1554 | 790 | 731 | 486 | 477 | 362 |
| -120 | 200 | 303 | 402 | 442 | 544 | 691 | 937 | 1211 | 1544 | 1232 | 1698 | 1336 | 1479 | 1409 | 991 | 757 | 677 | 488 | 410 | 299 | 331 |
| -160 | 262 | 320 | 319 | 506 | 442 | 651 | 1042 | 1217 | 1381 | 1238 | 1047 | 1610 | 1526 | 1473 | 915 | 758 | 453 | 641 | 332 | 264 | 313 |
| -200 | 231 | 246 | 344 | 453 | 381 | 627 | 544 | 1240 | 703 | 920 | 1058 | 998 | 918 | 853 | 686 | 505 | 612 | 592 | 324 | 299 | 210 |

(a) Fault normal

| M68(FP) | -400 | -360 | -320 | -280 | -240 | -200 | -160 | -120 | -80 | -40 | 00 | 40 | 80 | 120 | 160 | 200 | 240 | 280 | 320 | 360 | 40(km) |
|---|---|---|---|---|---|---|---|---|---|---|---|---|---|---|---|---|---|---|---|---|---|
| 200 | 332 | 354 | 471 | 548 | 429 | 571 | 559 | 702 | 765 | 735 | 972 | 895 | 708 | 702 | 641 | 603 | 647 | 688 | 495 | 393 | 354 |
| 160 | 338 | 436 | 538 | 712 | 759 | 747 | 971 | 756 | 1474 | 1127 | 1378 | 1454 | 1479 | 1221 | 828 | 909 | 707 | 799 | 612 | 418 | 427 |
| 120 | 364 | 418 | 546 | 615 | 811 | 844 | 1103 | 1362 | 1330 | 1543 | 1832 | 1781 | 1777 | 1267 | 1253 | 1168 | 963 | 803 | 602 | 497 | 392 |
| 80 | 501 | 607 | 867 | 1220 | 888 | 1009 | 981 | 2218 | 3145 | 2496 | 2800 | 2934 | 2068 | 1819 | 1759 | 1011 | 832 | 603 | 729 | 508 | 477 |
| 40 | 556 | 555 | 829 | 646 | 1146 | 972 | 1377 | 3230 | 2430 | 3105 | 3160 | 4659 | 3713 | 2131 | 1397 | 1182 | 1085 | 850 | 553 | 504 | 365 |
| 00 | 535 | 495 | 677 | 662 | 1020 | 1149 | 1338 | 2764 | 4235 | 3638 | 3035 | 5033 | 3471 | 2578 | 1547 | 1148 | 1037 | 909 | 622 | 532 | 366 |
| -40 | 571 | 481 | 863 | 1058 | 969 | 1132 | 1477 | 2215 | 3127 | 2995 | 2770 | 3061 | 2731 | 2219 | 1546 | 1188 | 806 | 1063 | 715 | 511 | 513 |
| -80 | 358 | 472 | 840 | 804 | 955 | 802 | 959 | 996 | 2097 | 1716 | 2421 | 1756 | 2884 | 1539 | 1672 | 1101 | 1008 | 865 | 713 | 476 | 483 |
| -120 | 360 | 484 | 702 | 596 | 625 | 892 | 715 | 899 | 1473 | 1279 | 1209 | 1454 | 1507 | 984 | 907 | 1189 | 783 | 605 | 599 | 609 | 337 |
| -160 | 393 | 465 | 464 | 1029 | 736 | 715 | 685 | 776 | 665 | 797 | 1427 | 855 | 1221 | 1298 | 576 | 632 | 635 | 920 | 589 | 485 | 464 |
| -200 | 306 | 433 | 482 | 607 | 525 | 441 | 477 | 542 | 711 | 640 | 727 | 944 | 614 | 751 | 623 | 426 | 691 | 531 | 506 | 541 | 386 |

(b) Fault parallel

(1) Hybrid technique ($f_{max}$=7.0Hz)

| M68sh | -400 | -360 | -320 | -280 | -240 | -200 | -160 | -120 | -80 | -40 | 00 | 40 | 80 | 120 | 160 | 200 | 240 | 280 | 320 | 360 | 40(km) |
|---|---|---|---|---|---|---|---|---|---|---|---|---|---|---|---|---|---|---|---|---|---|
| 200 | 383 | 434 | 483 | 540 | 606 | 681 | 764 | 849 | 929 | 993 | 1030 | 1030 | 992 | 925 | 841 | 753 | 670 | 595 | 530 | 474 | 426 |
| 160 | 405 | 457 | 514 | 582 | 665 | 762 | 875 | 999 | 1121 | 1224 | 1286 | 1289 | 1227 | 1117 | 987 | 859 | 745 | 649 | 569 | 503 | 448 |
| 120 | 425 | 477 | 542 | 622 | 721 | 847 | 1001 | 1183 | 1374 | 1534 | 1630 | 1640 | 1546 | 1368 | 1160 | 974 | 822 | 701 | 605 | 528 | 466 |
| 80 | 436 | 493 | 564 | 654 | 770 | 925 | 1131 | 1397 | 1671 | 1909 | 2079 | 2111 | 1944 | 1652 | 1347 | 1085 | 889 | 744 | 634 | 548 | 481 |
| 40 | 443 | 502 | 577 | 674 | 802 | 979 | 1233 | 1587 | 1994 | 2344 | 2614 | 2700 | 2414 | 1917 | 1495 | 1164 | 934 | 771 | 651 | 560 | 489 |
| 00 | 444 | 504 | 580 | 678 | 809 | 992 | 1258 | 1641 | 2114 | 2500 | 2805 | 2917 | 2581 | 1994 | 1528 | 1182 | 944 | 777 | 655 | 563 | 491 |
| -40 | 440 | 498 | 572 | 665 | 789 | 956 | 1188 | 1502 | 1833 | 2127 | 2347 | 2402 | 2180 | 1794 | 1432 | 1130 | 916 | 760 | 644 | 555 | 486 |
| -80 | 431 | 486 | 554 | 639 | 747 | 887 | 1067 | 1287 | 1520 | 1710 | 1838 | 1855 | 1731 | 1511 | 1254 | 1031 | 858 | 724 | 620 | 539 | 474 |
| -120 | 415 | 468 | 529 | 603 | 694 | 804 | 937 | 1087 | 1239 | 1371 | 1453 | 1459 | 1378 | 1235 | 1070 | 916 | 784 | 675 | 588 | 516 | 457 |
| -160 | 394 | 446 | 499 | 561 | 635 | 721 | 818 | 920 | 1019 | 1099 | 1147 | 1148 | 1100 | 1015 | 910 | 804 | 707 | 622 | 549 | 488 | 437 |
| -200 | 371 | 421 | 467 | 519 | 578 | 644 | 714 | 786 | 851 | 902 | 931 | 930 | 901 | 847 | 779 | 705 | 634 | 568 | 510 | 459 | 411 |

(2) Empirical approach

*Figure 9 Contour of estimated peak accelerations on seismic bedrock for $M_J$=6.8 with shallow fault and middle stress drop.*

| M73(FN) | -400 | -360 | -320 | -280 | -240 | -200 | -160 | -120 | -80 | -40 | 00 | 40 | 80 | 120 | 160 | 200 | 240 | 280 | 320 | 360 | 40(km) |
|---|---|---|---|---|---|---|---|---|---|---|---|---|---|---|---|---|---|---|---|---|---|
| 200 | 423 | 423 | 619 | 773 | 925 | 854 | 908 | 1086 | 979 | 1128 | 1153 | 1140 | 1027 | 1147 | 1231 | 1116 | 1339 | 1104 | 799 | 692 | 611 |
| 160 | 363 | 549 | 725 | 1133 | 943 | 1225 | 1008 | 1498 | 1740 | 1086 | 1411 | 1394 | 1335 | 1414 | 1189 | 1364 | 1607 | 1462 | 1323 | 834 | 761 |
| 120 | 722 | 596 | 987 | 934 | 961 | 1300 | 1412 | 1435 | 1720 | 1616 | 1668 | 1471 | 1563 | 1508 | 1680 | 1808 | 1775 | 1223 | 1374 | 1049 | 940 |
| 80 | 579 | 1198 | 1052 | 1309 | 1512 | 1393 | 1708 | 1438 | 1746 | 2139 | 2231 | 2189 | 1936 | 1846 | 2164 | 2088 | 1734 | 1927 | 1408 | 1394 | 1080 |
| 40 | 629 | 1372 | 1446 | 1417 | 1319 | 1557 | 1957 | 1897 | 2747 | 2176 | 2347 | 2537 | 2607 | 2338 | 2434 | 2263 | 2012 | 1946 | 1871 | 1283 | 1520 |
| 00 | 746 | 1132 | 1474 | 1476 | 1343 | 1600 | 1931 | 1988 | 2325 | 2369 | 2416 | 2565 | 3321 | 2241 | 2243 | 2617 | 2655 | 1840 | 1536 | 1411 | 1679 |
| -40 | 736 | 1313 | 1229 | 1225 | 1844 | 1572 | 1899 | 1723 | 2020 | 1909 | 2678 | 2226 | 2422 | 2243 | 1637 | 2428 | 2042 | 1521 | 2048 | 1456 | 1391 |
| -80 | 535 | 600 | 1022 | 913 | 1026 | 1309 | 1282 | 1254 | 1762 | 2652 | 1905 | 1842 | 1744 | 1429 | 2315 | 2125 | 2278 | 1610 | 1314 | 1059 | 1129 |
| -120 | 453 | 484 | 690 | 844 | 748 | 1162 | 1676 | 1230 | 1286 | 1431 | 1151 | 1550 | 1341 | 1762 | 1405 | 1452 | 1347 | 1196 | 1805 | 1271 | 612 |
| -160 | 468 | 568 | 670 | 766 | 1019 | 865 | 1011 | 1172 | 958 | 1248 | 1221 | 1068 | 1401 | 1595 | 1084 | 1090 | 1230 | 945 | 1064 | 683 | 664 |
| -200 | 434 | 525 | 605 | 536 | 644 | 792 | 830 | 897 | 1077 | 1277 | 1466 | 1122 | 1068 | 938 | 1171 | 1254 | 1144 | 815 | 941 | 703 | 852 |

(a) Fault normal

| M73(FP) | -400 | -360 | -320 | -280 | -240 | -200 | -160 | -120 | -80 | -40 | 00 | 40 | 80 | 120 | 160 | 200 | 240 | 280 | 320 | 360 | 40(km) |
|---|---|---|---|---|---|---|---|---|---|---|---|---|---|---|---|---|---|---|---|---|---|
| 200 | 470 | 656 | 599 | 816 | 840 | 701 | 864 | 830 | 894 | 1557 | 1391 | 1405 | 1375 | 1400 | 1066 | 1151 | 1112 | 888 | 819 | 959 | 1074 |
| 160 | 631 | 565 | 790 | 680 | 837 | 1266 | 1024 | 1100 | 1097 | 1935 | 2343 | 1419 | 1640 | 1522 | 1457 | 1977 | 1393 | 1320 | 776 | 984 | 974 |
| 120 | 507 | 696 | 736 | 1133 | 1288 | 1155 | 1268 | 1606 | 1521 | 1653 | 1869 | 1873 | 2056 | 1768 | 1606 | 1652 | 1493 | 1276 | 1128 | 859 | 1161 |
| 80 | 658 | 608 | 1087 | 1106 | 1619 | 1604 | 1731 | 1256 | 1730 | 1694 | 1374 | 2015 | 2039 | 2258 | 2210 | 2112 | 2457 | 1878 | 1745 | 890 | 1137 |
| 40 | 514 | 808 | 1372 | 1146 | 1065 | 1342 | 1419 | 1744 | 1726 | 1559 | 1842 | 2341 | 3084 | 2440 | 1935 | 2179 | 1904 | 1457 | 1218 | 1274 | 1120 |
| 00 | 573 | 677 | 1196 | 1174 | 1279 | 1538 | 1585 | 2111 | 2221 | 1472 | 1716 | 1988 | 1969 | 2783 | 2067 | 1991 | 2045 | 1477 | 1184 | 1618 | 1145 |
| -40 | 482 | 565 | 1228 | 1388 | 1509 | 1506 | 1395 | 1902 | 2745 | 1872 | 1779 | 1897 | 2316 | 1991 | 3130 | 2204 | 1808 | 1336 | 1331 | 1230 | 978 |
| -80 | 554 | 580 | 1117 | 1004 | 1226 | 1237 | 1882 | 1638 | 1656 | 1277 | 1386 | 1853 | 2166 | 2322 | 1877 | 2095 | 1364 | 1507 | 1029 | 977 | 890 |
| -120 | 692 | 795 | 591 | 735 | 997 | 1478 | 1281 | 1581 | 1762 | 1716 | 1808 | 1373 | 1325 | 2250 | 1817 | 1802 | 1309 | 1107 | 935 | 1138 | 858 |
| -160 | 622 | 542 | 799 | 686 | 1013 | 1382 | 1146 | 1343 | 1388 | 1827 | 1528 | 1649 | 1495 | 1699 | 1464 | 1390 | 1258 | 1381 | 1052 | 1356 | 832 |
| -200 | 583 | 555 | 601 | 680 | 724 | 920 | 672 | 828 | 973 | 862 | 1182 | 1397 | 1215 | 1138 | 1160 | 1117 | 1204 | 998 | 669 | 969 | 1163 |

(b) Fault parallel

(1) Hybrid technique ($f_{max}$=7.0Hz)

| M73sh | -400 | -360 | -320 | -280 | -240 | -200 | -160 | -120 | -80 | -40 | 00 | 40 | 80 | 120 | 160 | 200 | 240 | 280 | 320 | 360 | 40(km) |
|---|---|---|---|---|---|---|---|---|---|---|---|---|---|---|---|---|---|---|---|---|---|
| 200 | 678 | 747 | 824 | 908 | 995 | 1082 | 1165 | 1240 | 1308 | 1369 | 1419 | 1455 | 1468 | 1454 | 1407 | 1330 | 1232 | 1125 | 1018 | 918 | 828 |
| 160 | 716 | 799 | 894 | 1000 | 1113 | 1225 | 1330 | 1423 | 1504 | 1577 | 1643 | 1696 | 1723 | 1708 | 1645 | 1541 | 1409 | 1263 | 1122 | 995 | 885 |
| 120 | 752 | 849 | 966 | 1104 | 1254 | 1403 | 1531 | 1640 | 1734 | 1823 | 1911 | 1991 | 2039 | 2028 | 1942 | 1793 | 1606 | 1413 | 1228 | 1069 | 938 |
| 80 | 781 | 894 | 1036 | 1215 | 1422 | 1617 | 1779 | 1906 | 2009 | 2109 | 2220 | 2336 | 2417 | 2413 | 2298 | 2088 | 1824 | 1558 | 1325 | 1133 | 980 |
| 40 | 800 | 923 | 1087 | 1314 | 1605 | 1878 | 2073 | 2211 | 2314 | 2417 | 2544 | 2690 | 2805 | 2811 | 2670 | 2399 | 2039 | 1676 | 1394 | 1174 | 1007 |
| 00 | 804 | 930 | 1099 | 1342 | 1677 | 1986 | 2189 | 2328 | 2430 | 2532 | 2661 | 2815 | 2938 | 2947 | 2800 | 2513 | 2113 | 1707 | 1409 | 1183 | 1013 |
| -40 | 792 | 911 | 1065 | 1268 | 1513 | 1743 | 1924 | 2057 | 2162 | 2264 | 2385 | 2518 | 2617 | 2618 | 2489 | 2246 | 1935 | 1624 | 1365 | 1157 | 996 |
| -80 | 768 | 873 | 1002 | 1159 | 1335 | 1504 | 1649 | 1767 | 1866 | 1961 | 2061 | 2158 | 2222 | 2213 | 2114 | 1936 | 1713 | 1487 | 1279 | 1103 | 961 |
| -120 | 735 | 824 | 930 | 1050 | 1180 | 1309 | 1427 | 1526 | 1614 | 1694 | 1771 | 1837 | 1873 | 1859 | 1786 | 1661 | 1505 | 1337 | 1175 | 1033 | 912 |
| -160 | 697 | 773 | 858 | 952 | 1051 | 1150 | 1243 | 1327 | 1403 | 1469 | 1526 | 1569 | 1588 | 1573 | 1520 | 1432 | 1317 | 1192 | 1069 | 956 | 857 |
| -200 | 658 | 721 | 791 | 866 | 943 | 1020 | 1094 | 1161 | 1222 | 1275 | 1319 | 1349 | 1360 | 1345 | 1303 | 1237 | 1154 | 1062 | 969 | 880 | 799 |

1500 / 1500 1000 / 1000 500 / 500 400 / 400 / 300 300 / 200 200 / 100 100 / 50 / 10 10 / 0 / : Maximum value (Unit: cm/s$^2$)

(2) Empirical approach

*Figure 10 Contour of estimated peak accelerations on seismic bedrock for $M_J$=7.3 with shallow fault and middle stress drop.*

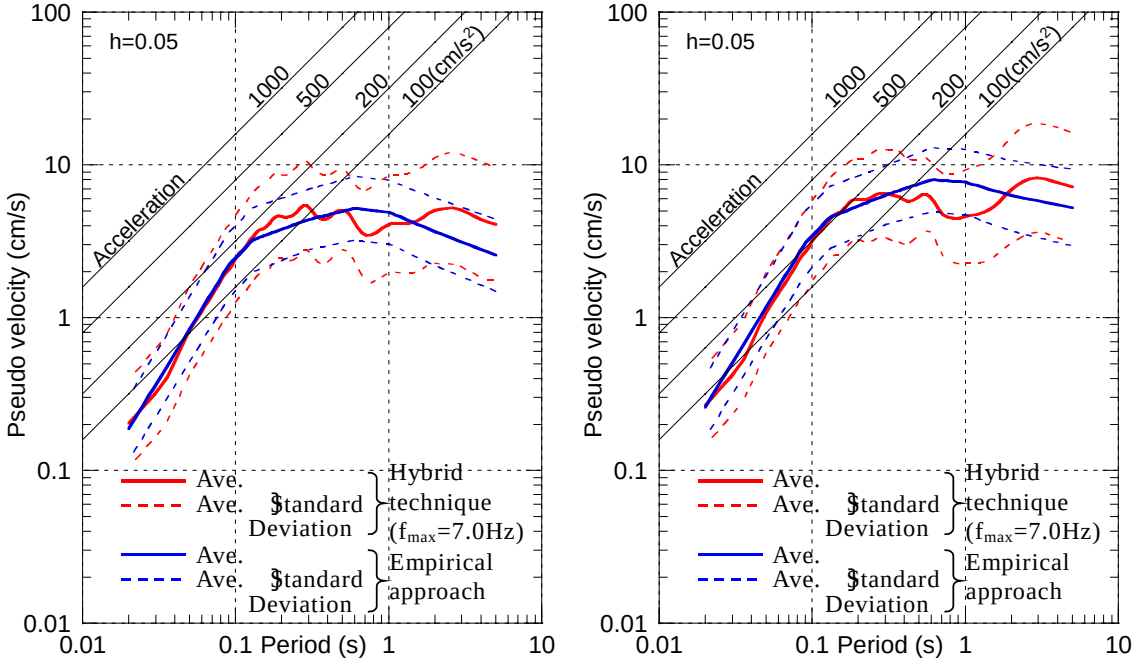


(1) $M_J$=6.5 (2) $M_J$=6.8

*Figure 11 Horizontal pseudo velocity response spectra on seismic bedrock evaluated by hybrid technique and empirical approach.*

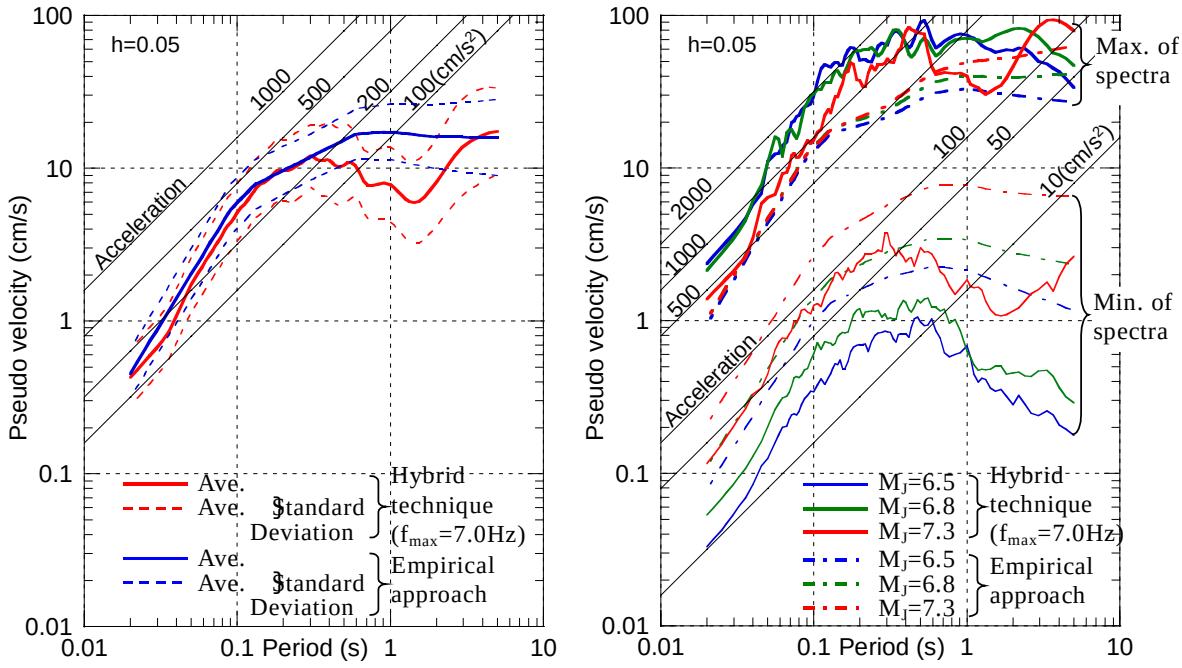


(3) $M_J$=7.3 (4) $M_J$=6.5, 6.8, and 7.3

*Figure 11 Horizontal-pseudo velocity response spectra on seismic bedrock evaluated by hybrid technique and empirical approach. (Continued).*

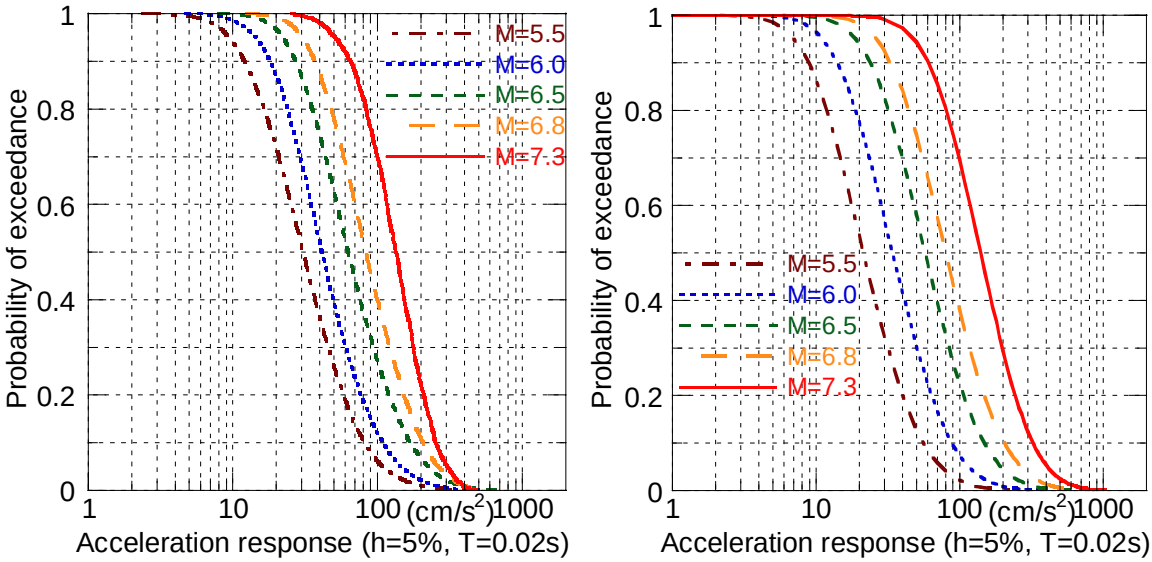


(1) Hybrid technique (2) Empirical approach

*Figure 12 Probability of exceedance of horizontal-acceleration response spectra (T=0.02 s) on seismic bedrock evaluated by hybrid technique and empirical approach.*

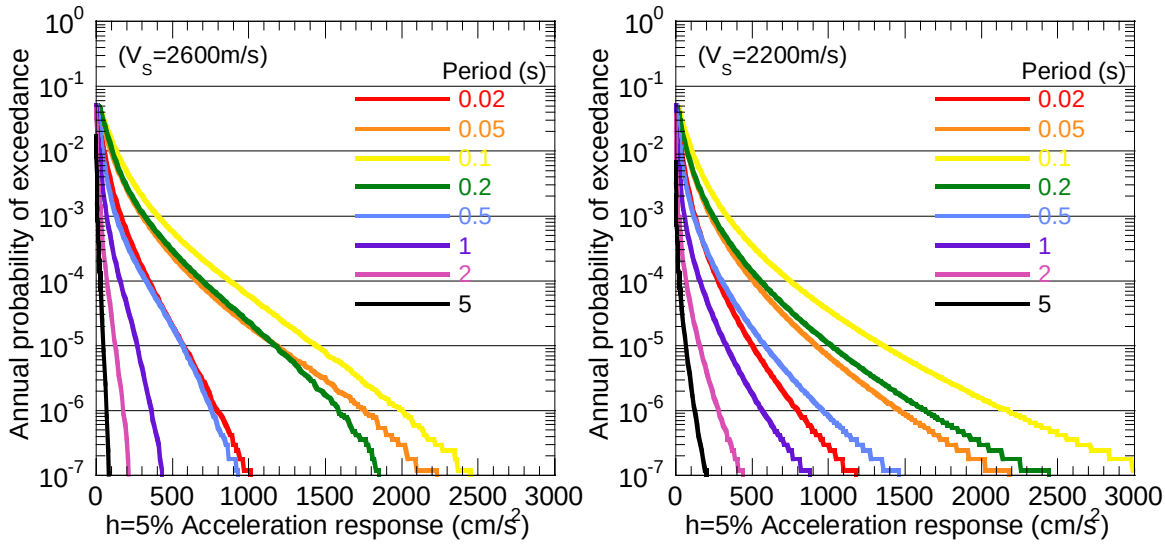


*Figure 13 Hazard curves of horizontal-acceleration response spectra on seismic bedrock evaluated by hybrid technique and empirical approach.*

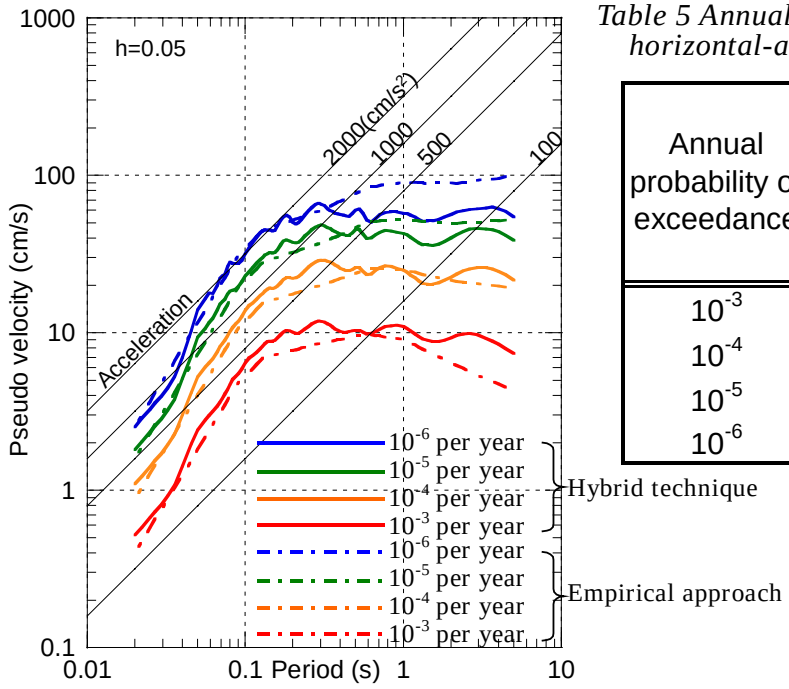


*Table 5 Annual probability of exceedance of horizontal-acceleration response spectra.*

| Annual probability of exceedance | Horizontal-acceleration response spectra (T=0.02 s) | |
|---|---|---|
| | Hybrid technique | Empirical approach |
| $10^{-3}$ | 160 cm/s$^2$ | 130 cm/s$^2$ |
| $10^{-4}$ | 340 cm/s$^2$ | 280 cm/s$^2$ |
| $10^{-5}$ | 570 cm/s$^2$ | 500 cm/s$^2$ |
| $10^{-6}$ | 800 cm/s$^2$ | 800 cm/s$^2$ |

*Figure 14 Uniform hazard spectra of the horizontal strong motion caused by buried-rupture earthquakes in evaluation area.*

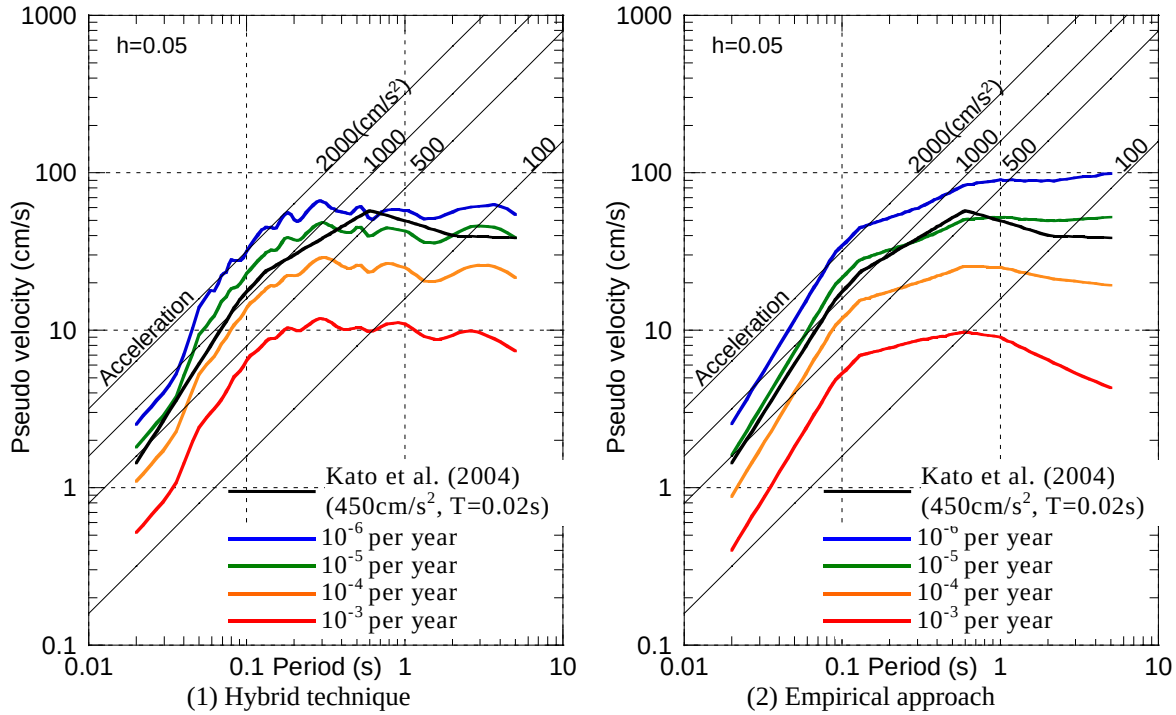


*Figure 15 Uniform hazard spectra of the horizontal strong motion caused by buried-rupture earthquakes and the upper level of the strong motion records proposed by Kato et al. (2004).*

## REFERENCES


Bouchon, M. (1981), "A Simple Method to Calculate Green's Function for Elastic Layered Media", Bulletin of the Seismological Society of America, Vol. 71, pp.959-971.

Dan, K., Kaneko, M., and Okumura, T. (2001), "Seismic Risk Analysis based on Strong Ground Motions Predicted by Fault Model", Programme and Abstracts, Seismological Society of Japan, 2001, Fall Meeting, P073 (in Japanese with English Abstract).

Irikura, K. and Miyake, H. (2001), "Prediction of Strong Ground Motions for Scenario Earthquakes", Journal of Geography, Vol. 110, No. 6, pp. 849-875 (in Japanese with English Abstract).

Kagawa, T. (2004), "Developing a Stochastic Green's Function Method Having More Accuracy in Long Period Range to be Used in the Hybrid Method", Journal of the Japan Association for Earthquake Engineering, Vol.4, 2, pp.21-32 (in Japanese with English Abstract).

Kagawa, T., Dan, K., Ohtsuka, Y., and Motohashi, S. (2005), "A Technique Setting Probability of Buried Rupture Earthquake for Probabilistic Earthquake Hazard Estimation", Japan Society of Civil Engineering, Journal of Earthquake Engineering, Vol.28 (in Japanese with English Abstract). (Submitted)

Kamae, K., Irikura, K., and Fukuchi, Y. (1990), "Prediction of Strong Ground Motion for M7 Earthquake Using Regional Scaling Relations of Source Parameters", Journal of the Structural and Construction Engineering (Transactions of the Architectural Institute of Japan), No.416, pp.57-70 (in Japanese with English Abstract).

Kamae, K., Irikura, K., and Pitarka, A. (1998), "A Technique for Simulating Strong Ground Motion Using Hybrid Green's Function", Bulletin of the Seismological Society of America, Vol.88, No.2, pp.357-367.

Kato, K., Miyakoshi, K., Takemura, M., Inoue, D., Ueta, K., and Dan, K. (2004), "Earthquake Ground Motions by Blind Faults in the Upper Crust – Categorization of Earthquakes Based on Geological Survey and Examination of the Upper Level from Strong Motion Records –", Journal of the Japan Association for Earthquake Engineering, Vol.4, 4, pp.46-86 (in Japanese with English Abstract).

Nishimura, I., Noda, S., Takahashi, K., Takemura, M., Ohno, S., Tohdo, M., and Watanabe, T. (2001), "Response Spectra for Design Purpose of Stiff Structures on Rock Sites", 16th International Conference on Structural Mechanics in Reactor Technology, K1133, pp.1-8.

Noda, S., Yashiro, K., Takahashi, K., Takemura, M., Ohno, S., Tohdo, M., and Watanabe, T. (2002), "Response Spectra for Design Purpose of Stiff Structures on Rock Sites", OECD-NEA Workshop on the Relations between Seismological Data and Seismic Engineering Analysis, pp.399-408.

Okada, Y. (1985), "Surface Deformation due to Shear and Tensile Faults in a Half-space", Bulletin of the Seismological Society of America, 75, pp.1135-1154.

Takemura, M. (1998), "Scaling Law for Japanese Intraplate Earthquakes in Special Relations to the Surface Faults and the Damages", Journal of the Seismological Society of Japan, Second Series, 51, pp.211-228 (in Japanese with English Abstract).


 